Increased intrusion of warming Atlantic water leads to rapid expansion of temperate phytoplankton in the Arctic

Griet Neukermans, Laurent Oziel, Marcel Babin

Increased intrusion of warming Atlantic water leads to rapid expansion of temperate phytoplankton in the Arctic

Griet Neukermans[1,2] | Laurent Oziel[1] | Marcel Babin[1]

[1]Takuvik Joint International Laboratory, CNRS, Université Laval, Québec, QC, Canada

[2]Sorbonne Université, CNRS, Laboratoire d'Océanographie de Villefranche-sur-Mer (LOV), F-Villefranche-sur-Mer, France

Correspondence
Griet Neukermans, Sorbonne Université, CNRS, Laboratoire d'Océanographie de Villefranche-sur-Mer (LOV), Villefranche-sur-Mer, France
Email: griet.neukermans@obs-vlfr.fr

Funding information
Horizon 2020 Framework Programme, Grant/Award Number: Marie Curie grant 749949; Natural Sciences and Engineering Research Council of Canada, Grant/Award Number: Banting Postdoctoral Fellowship, Canada Excellence Research Chair in Remote Sensing

Abstract

The Arctic Ocean and its surrounding shelf seas are warming much faster than the global average, which potentially opens up new distribution areas for temperate-origin marine phytoplankton. Using over three decades of continuous satellite observations, we show that increased inflow and temperature of Atlantic waters in the Barents Sea resulted in a striking poleward shift in the distribution of blooms of *Emiliania huxleyi*, a marine calcifying phytoplankton species. This species' blooms are typically associated with temperate waters and have expanded north to 76°N, five degrees further north of its first bloom occurrence in 1989. *E. huxleyi*'s blooms keep pace with the changing climate of the Barents Sea, namely ocean warming and shifts in the position of the Polar Front, resulting in an exceptionally rapid range shift compared to what is generally detected in the marine realm. We propose that as the Eurasian Basin of the Arctic Ocean further atlantifies and ocean temperatures continue to rise, *E. huxleyi* and other temperate-origin phytoplankton could well become resident bloom formers in the Arctic Ocean.

KEYWORDS
atlantification, biogeography, climate change, coccolithophore, *Emiliania huxleyi*, phytoplankton, range expansion, remote sensing

1 | INTRODUCTION

The most rapid and substantial climate driven changes in marine ecosystems are expected at high latitudes in regions within or bordering the Arctic Ocean where rates of warming are more than double the global average (Blunden, Arndt, Blunden, & Arndt, 2016). One such region is the Barents Sea (Figure 1), a highly productive Arctic shelf sea on the main northward path of Atlantic water into the Arctic Ocean (Smedsrud et al., 2013). Since 1980, the inflow of Atlantic waters into the Barents Sea has doubled (Oziel, Sirven, & Gascard, 2016) and warmed by 1.4°C (Figure 1), at a rate exceeding four times the global average (IPCC, 2013). In the last decade, temperatures hit highs not seen in a 110 years of recorded history (Boitsov, Karsakov, & Trofimov, 2012). The increased inflow of Atlantic waters is referred to as *atlantification* (sensu Årthun, Eldevik, Smedsrud, Skagseth, & Ingvaldsen, 2012; Oziel et al., 2016), which is thought to be the main cause for the dramatic loss of half of the winter sea ice cover in the area (Årthun et al., 2012) and a northeastward shift in the position of the temperature front (Oziel et al., 2016) where advected warm and saline Atlantic water meets southward flowing fresh and cold Arctic water (Figure 1). As a consequence of climate change, Atlantic waters thus carry nutrients and plankton further and further northeast in a continuous advective domain, creating trails of life or death for warmer-affinity species depending on whether organisms are able to survive and thrive in their new environments (Wassmann et al., 2015).

Phytoplankton, which form the foundation of the marine food web, are particularly responsive to climate change due to their short generation times, on the order of days, and being numerous and free-floating, so they rapidly track changing environmental conditions (Boyd, Strzepek, Fu, & Hutchins, 2010). Here, we investigate the response of the bloom-forming species *Emiliania huxleyi*, a cosmopolitan coccolithophore, omnipresent in all except the polar oceans (Winter, Jordan, & Roth, 1994). More specifically, we

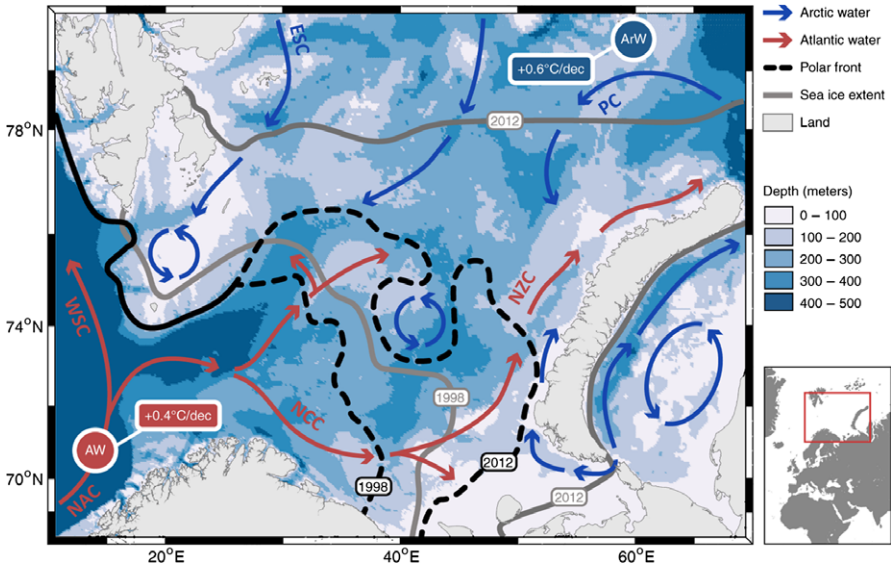

FIGURE 1 Conceptual scheme of increased inflow and warming of Atlantic water into the Barents Sea. Conditions of diminishing sea ice and Arctic water masses, depicted on a bathymetric background. Warming rates for surface waters in summer were computed over the period 1982–2014 (Table S1). Arrows indicate major currents (redrawn from the Norwegian Environment Agency). NAC, Norwegian Atlantic Current; WSC, West Spitzbergen Current; NCC, North Cape Current; NZC, Novaya Zemlya Current; PC, Persey Current; ESC, East Spitzbergen Current (after [Harris, Plueddemann, & Gawarkiewicz, 1998])

examine the recent suggestion that the species may be expanding its range into the polar oceans (Winter, Henderiks, Beaufort, Rickaby, & Brown, 2014) and its potential causes. *E. huxleyi* plays a crucial role in ocean biogeochemistry and various climate change feedback mechanisms. For example, *E. huxleyi* is known to alter the Earth's radiation budget (Tyrrell, Holligan, & Mobley, 1999), decrease oceanic CO_2 uptake through the reduction of surface layer alkalinity (Frankignoulle, Canon, & Gattuso, 1994) and may enhance carbon flux to depth by providing calcite ballast to sink organic particles (Riebesell et al., 2016).

Emiliania huxleyi is known to form extensive blooms in summer, especially in the temperate and subpolar Atlantic Ocean covering areas up to 250,000 km^2 (*e.g.* Holligan et al., 1993). Like all coccolithophores, *E. huxleyi* cells are covered by calcite plates or coccoliths, but *E. huxleyi* is unique in the sense that it overproduces coccoliths, which are released into the water at the final bloom stage (Paasche, 2001). The resulting accumulated *E. huxleyi* cells (typical densities $>10^9$ cells/m^3) and detached coccoliths in surface waters scatter so much light they turn seawater bright milky-turquoise, making these blooms easily detectable from space both by modern ocean colour satellites (1998–present) and by older and less sensitive optical satellite sensors (1982–present), such as the advanced very high-resolution radiometer, AVHRR (Smyth, Tyrell, & Tarrant, 2004).

To examine the poleward range expansion of *E. huxleyi* and the environmental conditions driving the range shift, we analyse a continuous, long-term (1982–present) dataset, which combines optical satellite observations of *E. huxleyi* blooms with satellite data of sea-surface temperature (SST), and other environmental parameters in the Barents Sea. We first investigate the intensity and distribution area of *E. huxleyi* summer blooms from remotely sensed particulate inorganic carbon concentration, PIC, derived from ocean colour satellites (1998–2016). In conjunction, we use remotely sensed SST data to locate the temperature front that separates Atlantic from Arctic water masses. We further extend the time series of *E. huxleyi* bloom areal distribution and SST back to the first bloom occurrence in 1989 using observations from the AVHRR optical sensor (Smyth et al., 2004) to quantify long-term shifts in the leading edge of *E. huxleyi's* bloom distribution.

2 | MATERIALS AND METHODS

2.1 | Remote sensing data

NASA's daily level 3 products from the SeaWiFS (1998–2007, 9.2 km spatial resolution) and MODIS (2003–2016, 4.6 km spatial resolution) ocean colour sensors were downloaded from NASA's ocean colour website (http://oceandata.sci.gsfc.nasa.gov) and included Chlorophyll-a concentration (Chl *a*), PIC, Photosynthetically available radiation (PAR) and euphotic zone depth (Z_{eu}). The ocean colour satellite PIC product is derived from NASA's standard PIC algorithm (Balch, Gordon, Bowler, Drapeau, & Booth, 2005; Gordon et al., 2001), which is based on a robust relationship between the light backscattering coefficient of particles suspended in seawater and the concentration of coccospheres and coccoliths, calcite plates forming the coccosphere of coccolithophores (Balch, Holligan, Ackleson, & Voss, 1991; Paasche, 2001). Some coccolithophore species, including *E. huxleyi*, shed excess coccoliths into the water during the later stages of a bloom (Paasche, 2001), creating large patches of highly reflective waters, which can be easily observed from space (Holligan et al., 1993). Satellite-derived PIC concentration provides a

good proxy for *E. huxleyi* calcite concentration in the Barents Sea because the coccolithophore population there is of low diversity and overwhelmingly dominated by *E. huxleyi* (Giraudeau et al., 2016). Furthermore, satellite PIC products have been successfully validated during *E. huxleyi* blooms in the Barents Sea (Burenkov, Kopelevich, Rat'kova, & Sheberstov, 2011; Giraudeau et al., 2016; Hovland, Dierssen, Ferreira, & Johnsen, 2013) and in other bloom areas (Balch et al., 2005; Holligan et al., 1993). The exclusion of PIC data in shallow coastal waters with bottom depth below 100 m helped minimize spurious high PIC concentrations caused by strong light backscattering from resuspended particles (Broerse et al., 2003) and excluded coastal fjords in which the coccolithophore population is more diverse than in offshore waters (Volent et al., 2011).

2.2 | Mixed-layer depth

Daily density-based estimates of mixed-layer depth at 0.25° spatial resolution were obtained from global ocean reanalysis products, GLORYS2v3, of the European Union Copernicus Marine Environment Monitoring Service (http://marine.copernicus.eu/). The reanalysis are built to be as close as possible to the observations (of altimetric sea level anomaly, temperature and salinity in situ profiles, sea-surface temperature observations, and sea ice concentration) and in agreement with the model physics.

2.3 | Water mass classification and validation

Classification of water masses from 1982 till 2014 was based on (i) remotely sensed daily sea-surface temperature at 4 km spatial resolution from the AVHRR sensor obtained through the National Oceanic and Atmospheric Administration (NOAA) (Baker-Yeboah et al., 2016) and (ii) sea ice concentration at 25 km spatial resolution from the Special Sensor Microwave Imager (SSMI) (1998–2007) and SSMI/Sounder (2008–2014) sensors obtained through the National Snow and Ice Data Center (NSIDC) (Cavalieri, Parkinson, Gloersen, & Zwally, 1996). To determine the position of the Polar Front, which separates warm Atlantic waters from cold Arctic waters, we performed a local variance filter with a window size of 7 × 7 pixels on the March–April mean SST data. This time window optimizes remotely sensed SST data availability at a time the water column is vertically well mixed and well before Atlantic waters thermally stratify. The position of the Polar Front is seasonally stable (Figure S1); therefore, the position of the SST front in March–April is a good indicator for the annual extent of Atlantic waters. A histogram of pixels where the standard deviation exceeded the absolute value of the mean SST within the moving window was built and the Polar Front waters, PFW, were defined as those pixels that had SST between the 16^{th} and 84^{th} percentiles of the corresponding histogram of SST values (Oziel et al., 2016). Over the 1982–2014 period, the lower and upper SST bounds of Polar Front waters were rather stable with respective mean values (±standard deviation) of −0.47°C (±0.07°C) and 0.50°C (±0.09°C) (Table S2). Six water masses were derived as follows: (i) North Atlantic waters, NAW, with March–April mean SST above 3°C (Loeng, 1991), (ii) Modified Atlantic Waters, MAW, between NAW and PFW, (iii) PFW with temperature ranges shown in Table S2, (iv) the seasonal ice zone, SIZ, with maximum winter sea ice extent above 80% and summer minimum extent below 20%, (v) the perennial ice covered waters, PIW, with summer minimum ice cover above 20% and (vi) Arctic Waters, ArW, between the SIZ and the PFW. If no March–April mean SST data were available in ice-free waters due to persistent cloudiness, pixels were considered unclassified, which was the case for less than 5% of the Barents Sea coverage (Figure S2). The remote sensing-based classification of water masses was validated using a collection of hydrographic in situ data with over 130,000 profiles of temperature and salinity collected between 1980 and 2012 (Figure S3).

3 | RESULTS

Our analyses of the intensity and distribution area of *E. huxleyi* summer blooms (1998–2016) in conjunction with water mass distribution show that *E. huxleyi* blooms are confined to Atlantic waters and closely track the position of the temperature front (Figure 2). The front has strongly shifted northeastward commensurate with a doubling in areal coverage of Atlantic water over the study period from 10% in 1998 to 23% in 2014 and alongside a strong reduction in the areal coverage of Arctic waters from 60% to 30% (Figure S2). In the Eastern Barents Sea, the leading edge of *E. huxleyi*'s bloom distribution has shifted northward by 3° latitude, equivalent to 20.5 km per year over the period 1998–2016 (Figure 3).

Extending the time series of *E. huxleyi* bloom areal distribution back to the first bloom occurrence in 1989 (Smyth et al., 2004) gives a northward shift of the leading edge of 501 km in nearly 30 years (Figure 3; Table S3). The rate of range shift has clearly accelerated in the present decade (56 km per year in 2010–2016), in pace with the accelerated northward shift of the Polar Front. Moreover, three out of four of the most expansive blooms on record occurred in the present decade (2011–2012, and 2016, Figure 2; Figure S4).

4 | DISCUSSION

Poleward expansions at the leading edges of marine species have been observed across all ocean regions with global average rate of 72 ± 13 km per decade (Poloczanska et al., 2013, 2016), as expected for biological and ecological responses to ocean warming. Fastest leading-edge expansions were seen for highly mobile or dispersive pelagic organisms such as bony fish (278 ± 77 km per decade), invertebrate zooplankton (142 ± 28 km per decade) and phytoplankton (358 km ± 68 per decade). Here, we quantify for the first time the rate of poleward range shift of *E. huxleyi*, the most abundant and productive coccolithophore species. In contrast to the two phytoplankton range shifts reported in a recent meta-analysis (310 km per decade for *Ceratium trichoceros*; 406 km per decade for *Noctiluca scintillans*) (Poloczanska et al., 2013, 2016), our analyses

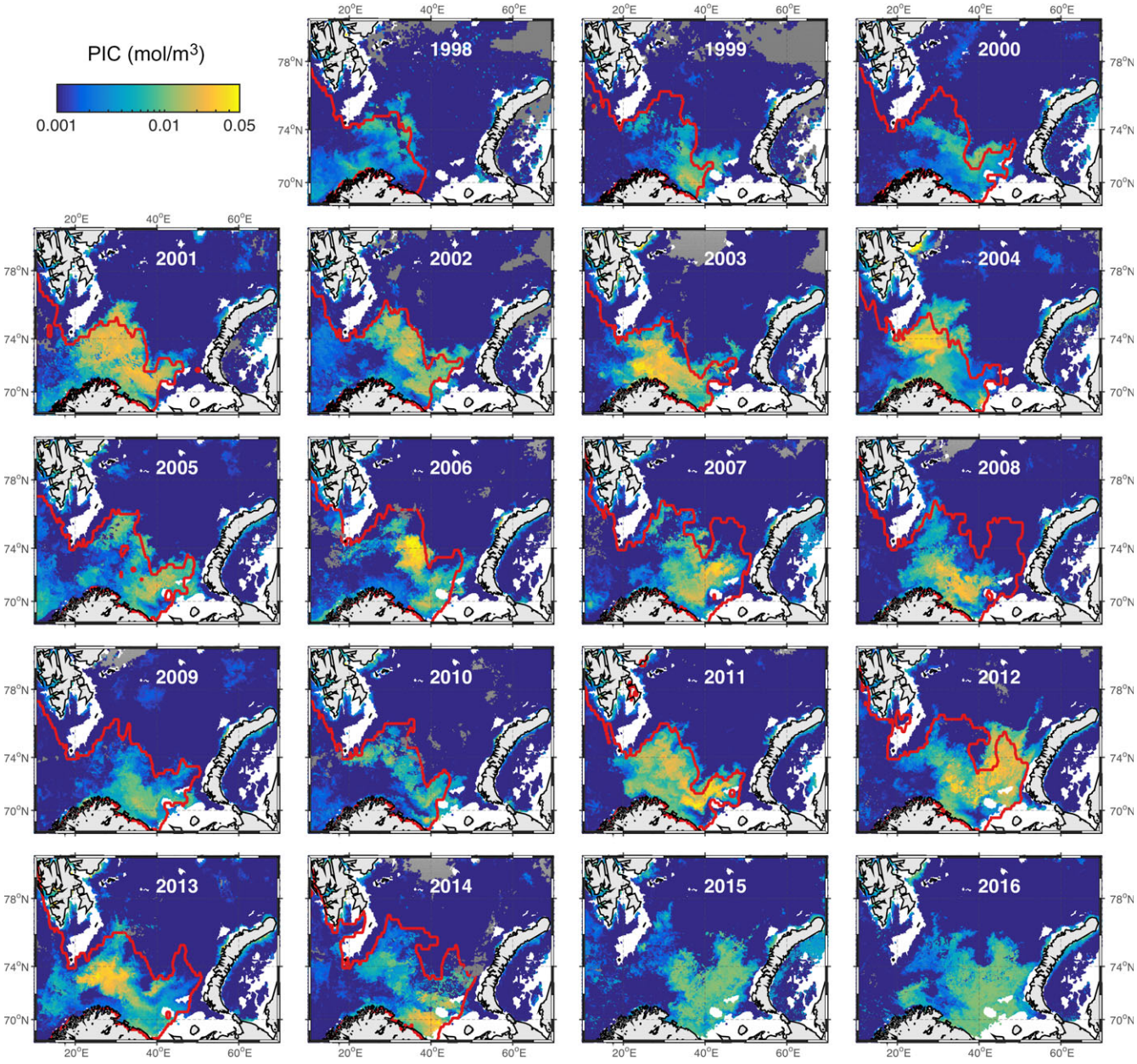

FIGURE 2 Time series of *Emiliania huxleyi* bloom calcite concentration and areal extent. Summer maximum calcite concentration in the Barents Sea was obtained from SeaWiFS (1998–2002) and MODIS (2003–2016) ocean colour satellite sensors. Red line delineates the extent of Atlantic waters (1998–2014). Areas shallower than 150 m were masked in white and no data in grey

are based on continuous long-term synoptic observations of areal distribution and bloom magnitude at spatiotemporal scales unattainable by traditional ship-based sampling.

We propose that the recent rapid expansion of *E. huxleyi* blooms in the Barents Sea is triggered by concurrent increases in the areal extent and temperature of Atlantic waters. On the one hand, plankton and nutrients propagate further northeast, while on the other hand rising temperature of Atlantic water in the Barents Sea has created an environment in which *E. huxleyi* is able to form extensive blooms since the late 1980s, with an interruption in the mid-1990s due to colder water temperature (Smyth et al., 2004) (Figure S5). Changing water masses and fronts has also facilitated plankton shifts in other ocean regions when accompanied by increasing ocean temperature (Poloczanska et al., 2016), which allows marine organisms to survive and thrive in new environments.

Our observations highlight two distinct barriers to *E. huxleyi* dispersal. First, blooms were exclusively found in Atlantic waters, suggesting that the Polar Front represents a physical barrier to dispersal (Figure 2). Second, no blooms were detected in Atlantic waters with summer mean sea-surface temperature below 6°C, suggesting a thermal barrier to bloom occurrence. This is exemplified in Figure 4, which contrasts observations of 1998 and 2012 corresponding to minimal and maximal Atlantic water extent, respectively (Figure S2). In 1998, no *E. huxleyi* bloom was observed in Arctic waters even if

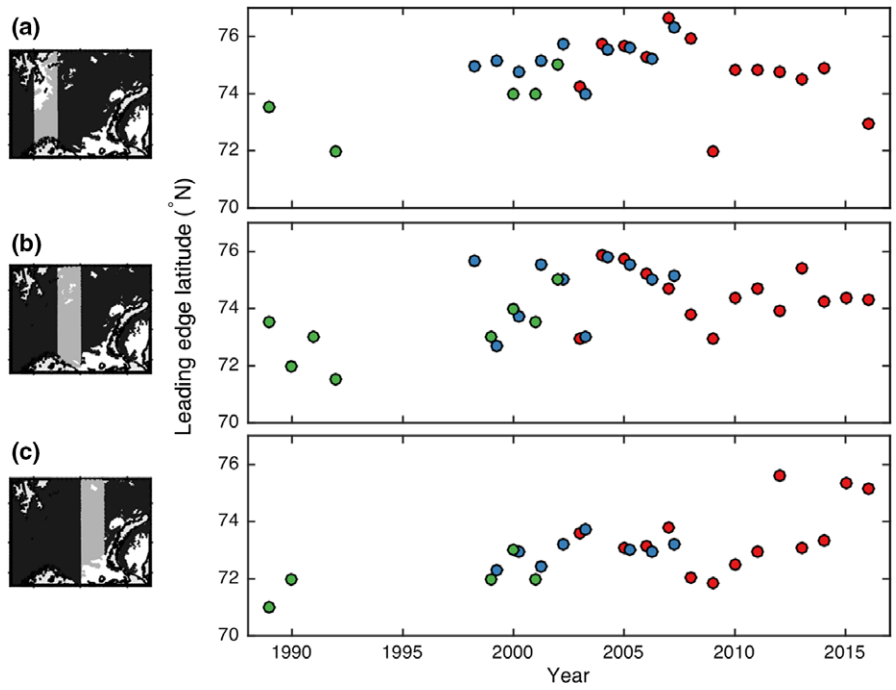

FIGURE 3 Shifting position of the leading edge of *Emiliania huxleyi* bloom distribution from 35 years of remote sensing data (1982–2016) for three longitude bands in the Barents Sea. (a) 20°E–30°E, (b) 30°E–40°E, (c) 40°E–50°E. Bloom areal coverage was obtained from a continuous record of optical satellite data, including the advanced very high-resolution radiometer (AVHRR) sensor (Smyth et al., 2004) (green), from which the first conspicuous bloom was detected in 1989, and the SeaWiFS (blue) and MODIS (red) ocean colour sensors

the summer mean sea-surface temperature was >6°C, whereas in 2012, no blooms were detected in waters with summer mean sea-surface temperature <6°C even if they were of Atlantic origin. A minimum summer SST of 6°C in Atlantic water appears to be conducive to *E. huxleyi* blooms (Figure 5a; Figure S6). This is consistent with experimental data on the temperature dependency of *E. huxleyi* maximum growth rates, which exhibits a similarly stark rise at a temperature of 6°C. Indeed, maximum growth rates in the 2−5°C temperature range are on the order of 0.1 per day and then jump to 0.5 per day at 6°C, beyond which growth rates increases as a power function of temperature (Fielding, 2013). Polar diatoms and other cold-water adapted phytoplankton have typical growth rates above 0.5 per day in the −1 to 5°C range, thus outcompeting *E. huxleyi* in cold waters (Lacour, Larivière, & Babin, 2017). Compared to bottom-up processes, top-down control of *E. huxleyi* blooms is thought to be of limited importance as it has been shown that calcification is an effective strategy to reduce grazer growth by creating indigestion or prolonging digestion time, resulting in net growth of *E. huxleyi* (Harvey, Bidle, & Johnson, 2015; Kolb & Strom, 2013; Monteiro et al., 2016).

The northern limit of *E. huxleyi* blooms in a warming Barents Sea is thus set by the position of the Polar Front, which is associated with a strong gradient in water temperature, and across which there is little exchange between Atlantic and Arctic water masses. However, as Arctic surface waters continue to warm at an average rate of 0.6°C per decade and Atlantic waters at a slightly slower rate of 0.4°C per decade (Figure S7; Table S1), we expect that the temperature front will weaken throughout the century. By the end of the century, *E. huxleyi* may start forming blooms in Arctic water masses, which will then be pushed northward of 82°N (Wassmann et al., 2015). Furthermore, it has been hypothesized that the Barents Sea will further atlantify through a self-amplifying positive feedback loop in which increased Atlantic water inflow enhances sea ice melt and anomalous cyclonic winds, which lead to an amplification of Atlantic water inflow (Smedsrud et al., 2013). We can therefore expect *E. huxleyi* blooms to expand further north along with Atlantic water masses. This is also supported by geological studies that revealed the presence of *E. huxleyi* in the Arctic Ocean during conditions of diminished sea ice and increased Atlantic inflow of past interglacial times (Backman, Fornaciari, & Rio, 2009) although we acknowledge that presence does not imply blooms.

Besides Atlantic water extent and water temperature, northward shifts of *E. huxleyi* will be constrained by other environmental conditions such as the strong seasonality of day length in the high Arctic and associated short annual window for phytoplankton growth (Kaartvedt, 2008), water column stability and nutrient availability (Tyrrell & Merico, 2004). The extreme light conditions in the high North, however, do not appear to be a limitation for *E. huxleyi* as viable populations have been found in Atlantic water north of Svalbard (>80°N) (Hegseth & Sundfjord, 2008) and laboratory experiments have shown the species' tolerance to low as well as high light, suggesting its capacity for survival in the high Arctic. Shallow mixed layers between 10 and 20 m are known to favour *E. huxleyi* blooms (Tyrrell & Merico, 2004), consistent with our observations of significant negative correlation between *E. huxleyi* bloom magnitude and summer mixed-layer depth which ranged between 10.5 and 19 m

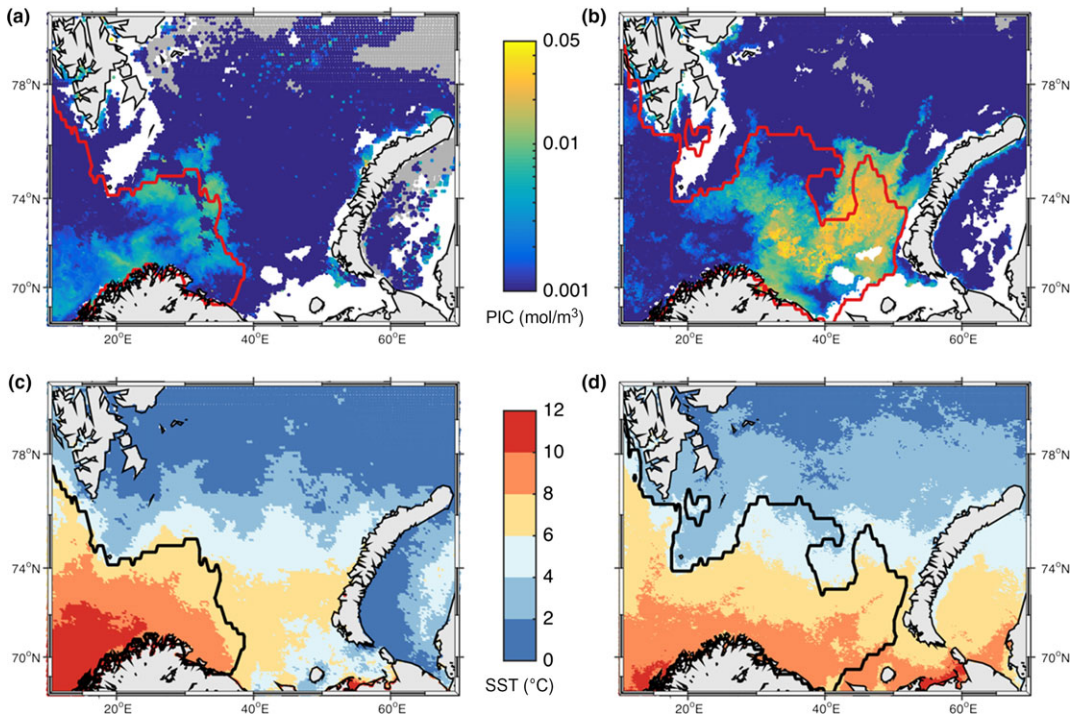

FIGURE 4 Physical and thermal barriers to dispersal of *Emiliania huxleyi* blooms in the Barents Sea. Exemplified in two contrasting years, 1998 (a, c) and 2012 (b, d). Remotely sensed *E. huxleyi* bloom magnitude in summer (a, b) indicate that *E. huxleyi* blooms in Atlantic waters delineated by the red line, with summer mean temperatures >6°C (c, d)

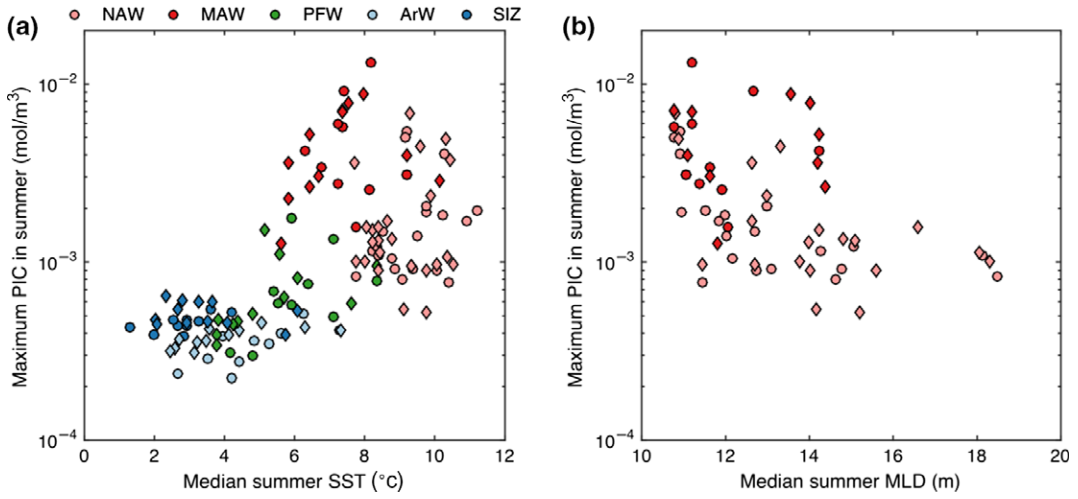

FIGURE 5 Environmental controls of *Emiliania huxleyi* bloom magnitude in the Barents Sea. Ocean colour satellite-derived *E. huxleyi* bloom magnitude in different water masses (see Methods) vs. (a) median summer sea-surface temperature (SST) and (b) median depth of the mixed layer in summer from SeaWiFS (circles) and MODIS (diamonds) ocean colour sensors

($r = -0.51 \pm 0.16$, $p = .00003$; Figure 5b; Table S4). Such mixed-layer depths are typical for the Arctic Ocean in summer (Peralta-Ferriz & Woodgate, 2015), thereby favouring northward expansion of *E. huxleyi* blooms. Due to its high nutrient affinity, *E. huxleyi* also performs well in nutrient-depleted environments and therefore blooms often occur after the demise of the diatom spring bloom (Iglesias-Rodríguez et al., 2002), such as observed in the Barents Sea in summer (Oziel et al., 2017). Since the early 1990s, nutrient stocks in the Atlantic water of the Barents Sea have gradually declined, particularly silicates which are experiencing a much larger decrease than nitrates (Rey, 2012). Such conditions are favourable for *E. huxleyi* at the expense of diatoms and modelling studies suggest that nutrient concentrations will continue to decline in the Arctic Ocean throughout this century, due to shoaling of the mixed layer and decreasing nutrients in the advected North Atlantic and Pacific waters (Slagstad, Wassmann, & Ellingsen, 2015; Vancoppenolle et al., 2013).

The expansion and warming of Atlantic water masses in the Barents Sea and the associated transport and thriving of Atlantic-origin

phytoplankton is expected to affect the entire marine food web. Warm-water species such as *E. huxleyi* tend to be smaller and less energy-rich than polar species. Indeed, an atlantification of marine organisms at higher trophic levels has also been reported in the Barents Sea, along with a poleward retraction of cold-water species (e.g. Fossheim et al., 2015). This suggests that *E. huxleyi* blooms can serve as early warnings of impending effects on the marine food web. Furthermore, it is expected that other temperate-origin phytoplankton species, including harmful ones, may also progress northward as temperatures within polar and subpolar regions become more permissive for species from lower latitudes (Gobler et al., 2017). Indeed, in the Bering Sea, *E. huxleyi* bloom occurrences have been considered harbingers of blooms of the toxic temperate-origin dinoflagellate *Alexandrium tamarense* (Walsh et al., 2011). This dinoflagellate has also become increasingly prevalent in waters off northern Norway since the late 1990s, whereas it was rare before (Walsh et al., 2011).

We note that there is a second route along which Atlantic-origin species may expand poleward into the Arctic Ocean as Atlantic waters flow northward through the wide and deep Fram Strait on the West Spitzbergen Current (WSC, Figure 1), which subducts and, north of Svalbard, turns eastwards and continues along the continental slope. In recent years, the influence of Atlantic waters along the WSC has also increased (Walczowski, Piechura, Goszczko, & Wieczorek, 2012), even extending into the eastern Eurasian Basin (atlantification sensu Polyakov et al., 2017). Many studies have reported increased importance of Atlantic species and atlantification of the marine food web west and north of Svalbard (Berge, Johnsen, Nilsen, Gulliksen, & Slagstad, 2005; Hegseth & Sundfjord, 2008; Ormańczyk, Głuchowska, Olszewska, & Kwasniewski, 2017; Wassmann et al., 2015; Węsławski, Buchholz, Głuchowska, & Weydmann, 2017). One in situ study in the summer of 2003 reported that *E. huxleyi* bloomed and dominated the phytoplankton assemblage in Atlantic waters that surfaced north of Svalbard (80–81°N, 30°E) with cell numbers up to $10^8/m^3$ (Hegseth & Sundfjord, 2008). Such occurrences of *E. huxleyi* blooms were not included in the present study because of prevailing low sun elevation at those latitudes and lower concentrations of *E. huxleyi* there. However, our analyses indicate that *E. huxleyi* does form blooms in the surface waters of the WSC southwest of Svalbard (Figures 2 and 5a), but they are weaker in intensity possibly due to a deeper summer mixed layer in the waters off the shelf (Figure 5b). This suggests that the dominance and blooming of *E. huxleyi* associated with atlantification may extend beyond the Barents Sea shelf. Furthermore, we expect that shoaling of Atlantic waters and decreased vertical stratification increasingly observed throughout the Eurasian Basin (atlantification sensu Polyakov et al., 2017) will favour the expansion of Atlantic-origin phytoplankton by decreasing their time spent in darkness and promoting their transport to surface waters.

In conclusion, using over three decades of continuous satellite observations, we provide evidence that *E. huxleyi* blooms have expanded poleward by 501 km since first occurrence in the Barents Sea in 1989 (Smyth et al., 2004). This northward range shift, which reached speeds up to 56 km per year in the present decade, represents one of the most rapid poleward expansions of marine organisms reported so far (Poloczanska et al., 2013, 2016). We show that *E. huxleyi's* blooms keep pace with the speed of local climate velocities (sensu Pinsky, Worm, Fogarty, Sarmiento, & Levin, 2013); closely tracking increasing temperatures and the shifting position of the Polar Front that separates Atlantic from Arctic waters. *E. huxleyi* blooms, which can be easily observed from space, thus testify of the encroaching atlantification of the Barents Sea (Årthun et al., 2012; Oziel et al., 2016) and may be considered as harbingers of cascading effects on the entire food web (Dalpadado et al., 2012; Fossheim et al., 2015) and of blooms of toxic temperate-origin phytoplankton (Walsh et al., 2011). We propose that as the Eurasian Basin of the Arctic Ocean further atlantifies (Polyakov et al., 2017) and Atlantic Ocean temperatures continue to rise, *E. huxleyi* and other temperate-origin phytoplankton (including harmful species), could well become resident bloom formers in the Arctic Ocean.

ACKNOWLEDGEMENTS

We thank NASA Ocean Biology Processing Group and the NSIDC for providing ocean colour and sea ice concentration satellite data, respectively. We thank E. Devred for downloading and reprojecting AVHRR SST data provided by the GHRSST and the US National Oceanographic Data Center, T. Jessin for designing Figure 1, and D. Slagstad for providing the SINMOD model. We further thank E. Rehm and M. Benoit-Gagné for programming support and T. Smyth for providing a high-resolution version of Figure 2 in Smyth et al. (2004). G.N. was supported by a Banting Postdoctoral Fellowship from the Government of Canada (2015–2017) and by a European Union's Horizon 2020 Marie Sklodowska-Curie grant (no. 749949). Finally, we thank Ulf Riebesell, Maurice Levasseur, Geir Johnsen, Luc Beaufort and Hervé Claustre for feedback on our manuscript.

ORCID

Griet Neukermans http://orcid.org/0000-0002-8258-3590

REFERENCES

Årthun, M., Eldevik, T., Smedsrud, L. H.Skagseth, Ø., & Ingvaldsen, R. B. (2012). Quantifying the influence of atlantic heat on barents sea ice variability and retreat. *Journal of Climate*, *25*, 4736–4743. https://doi.org/10.1175/jcli-d-11-00466.1

Backman, J., Fornaciari, E., & Rio, D. (2009). Biochronology and paleoceanography of late Pleistocene and Holocene calcareous nannofossil abundances across the Arctic Basin. *Marine Micropaleontology*, *72*, 86–98. https://doi.org/10.1016/j.marmicro.2009.04.001

Baker-Yeboah, S., Saha, K., Zhang, D., Casey, K. S., Kilpatrick, K. A., Evans, R. H., & Ryan, T. (2016). *AVHRR Pathfinder version 5.3 level 3 collated (L3C) global 4 km sea surface temperature*.

Balch, W. M., Gordon, H. R., Bowler, B. C., Drapeau, D. T., & Booth, E. S. (2005). Calcium carbonate measurements in the surface global ocean based on moderate-resolution imaging spectroradiometer data. *Journal of Geophysical Research*, *110*, C07001.

Balch, W. M., Holligan, P. M., Ackleson, S. G., & Voss, K. J. (1991). Biological and optical properties of mesoscale coccolithophore blooms in the Gulf of Maine. *Limnology and Oceanography*, *36*, 629–643. https://doi.org/10.4319/lo.1991.36.4.0629

Berge, J., Johnsen, G., Nilsen, F., Gulliksen, B., & Slagstad, D. (2005). Ocean temperature oscillations enable reappearance of blue mussels Mytilus edulis in Svalbard after a 1000 year absence. *Marine Ecology Progress Series*, *303*, 167–175. https://doi.org/10.3354/meps303167

Blunden, J., Arndt, D. S., Blunden, J., & Arndt, D. S. (2016). State of the climate in 2015. *Bulletin of the American Meteorological Society*, *97*, Si-S275.

Boitsov, V. D., Karsakov, A. L., & Trofimov, A. G. (2012). Atlantic water temperature and climate in the Barents Sea, 2000-2009. *ICES Journal of Marine Science*, *69*, 833–840. https://doi.org/10.1093/icesjms/fss075

Boyd, P. W., Strzepek, R., Fu, F., & Hutchins, D. A. (2010). Environmental control of open-ocean phytoplankton groups: Now and in the future. *Limnology and Oceanography*, *55*, 1353–1376. https://doi.org/10.4319/lo.2010.55.3.1353

Broerse, A. T., Tyrrell, T., Young, J., Poulton, A., Merico, A., Balch, W., & Miller, P. (2003). The cause of bright waters in the Bering Sea in winter. *Continental Shelf Research*, *23*, 1579–1596. https://doi.org/10.1016/j.csr.2003.07.001

Burenkov, V. I., Kopelevich, O. V., Rat'kova, T. N., & Sheberstov, S. V. (2011). Satellite observations of the coccolithophorid bloom in the Barents Sea. *Oceanology*, *51*, 766–774. https://doi.org/10.1134/s0001437011050043

Cavalieri, D., Parkinson, C., Gloersen, P., & Zwally, H. (1996). *Sea Ice Concentrations from Nimbus-7 SMMR and DMSP SSM/I-SSMIS Passive Microwave Data, Version 1*.

Dalpadado, P., Ingvaldsen, R. B., Stige, L. C., Bogstad, B., Knutsen, T., Ottersen, G., & Ellertsen, B. (2012). Climate effects on Barents Sea ecosystem dynamics. *ICES Journal of Marine Science*, *69*, 1303–1316. https://doi.org/10.1093/icesjms/fss063

Fielding, S. R. (2013). *Emiliania huxleyi* specific growth rate dependence on temperature. *Limnology and Oceanography*, *58*, 663–666. https://doi.org/10.4319/lo.2013.58.2.0663

Fossheim, M., Primicerio, R., Johannesen, E., Ingvaldsen, R. B., Aschan, M. M., & Dolgov, A. V. (2015). Recent warming leads to a rapid borealization of fish communities in the Arctic. *Nature Climate Change*, *5*, 673–677. https://doi.org/10.1038/nclimate2647

Frankignoulle, M., Canon, C., & Gattuso, J.-P. (1994). Marine calcification as a source of carbon dioxide: Positive feedback of increasing atmospheric CO_2. *Limnology and Oceanography*, *39*, 458–462. https://doi.org/10.4319/lo.1994.39.2.0458

Giraudeau, J., Hulot, V., Hanquiez, V., Devaux, L., Howa, H., & Garlan, T. (2016). A survey of the summer coccolithophore community in the western Barents Sea. *Journal of Marine Systems*, *158*, 93–105. https://doi.org/10.1016/j.jmarsys.2016.02.012

Gobler, C. J., Doherty, O. M., Hattenrath-Lehmann, T. K., Griffith, A. W., Kang, Y., & Litaker, R. W. (2017). Ocean warming since 1982 has expanded the niche of toxic algal blooms in the North Atlantic and North Pacific oceans. *Proceedings of the National Academy of Sciences*, *114*, 201619575.

Gordon, H. R., Boynton, G. C., Balch, W. M., Groom, S. B., Harbour, D. S., & Smyth, T. J. (2001). Retrieval of coccolithophore calcite concentration from SeaWiFS Imagery. *Geophysical Research Letters*, *28*, 1587–1590. https://doi.org/10.1029/2000gl012025

Harris, C. L., Plueddemann, A. J., & Gawarkiewicz, G. G. (1998). Water mass distribution and polar front structure in the western Barents Sea. *Journal of Geophysical Research: Oceans*, *103*, 2905–2917. https://doi.org/10.1029/97jc02790

Harvey, E. L., Bidle, K. D., & Johnson, M. D. (2015). Consequences of strain variability and calcification in Emiliania huxleyi on microzooplankton grazing. *Journal of Plankton Research*, *37*, fbv081. https://doi.org/10.1093/plankt/fbv081

Hegseth, E. N., & Sundfjord, A. (2008). Intrusion and blooming of Atlantic phytoplankton species in the high Arctic. *Journal of Marine Systems*, *74*, 108–119. https://doi.org/10.1016/j.jmarsys.2007.11.011

Holligan, P. M., Fernández, E., Aiken, J., Balch, W. M., Boyd, P., Burkill, P. H, … Purdie, D. A. (1993). A biogeochemical study of the coccolithophore, Emiliania huxleyi, in the North Atlantic. *Global Biogeochemical Cycles*, *7*, 879–900. https://doi.org/10.1029/93gb01731

Hovland, E. K., Dierssen, H. M., Ferreira, A. S., & Johnsen, G. (2013). Dynamics regulating major trends in Barents Sea temperatures and subsequent effect on remotely sensed particulate inorganic carbon. *Marine Ecology Progress Series*, *484*, 17–32. https://doi.org/10.3354/meps10277

Iglesias-Rodríguez, M. D., Brown, C. W., Doney, S. C., Kleypas, J., Kolber, D., Kolber, Z., … Falkowski, P. G. (2002). Representing key phytoplankton functional groups in ocean carbon cycle models: Coccolithophorids. *Global Biogeochemical Cycles*, *16*(4), 1100. https://doi.org/10.1029/2001GB001454

IPCC. (2013). Climate change 2013: The physical science basis. In T. F. Stocker, D. Qin, G.-K. Plattner, M. Tignor, S. K. Allen, J. Boschung, A. Nauels, Y. Xia, V. Bex & P. M. Midgley (Eds.), *Contribution of working group I to the fifth assessment report of the intergovernmental panel on climate change* (pp. 1535). Cambridge, United Kingdom and New York, NY, USA: Cambridge University Press.

Kaartvedt, S. (2008). Photoperiod may constrain the effect of global warming in arctic marine systems. *Journal of Plankton Research*, *30*, 1203–1206. https://doi.org/10.1093/plankt/fbn075

Kolb, A., & Strom, S. (2013). An inducible antipredatory defense in haploid cells of the marine microalga *Emiliania huxleyi* (Prymnesiophyceae). *Limnology and Oceanography*, *58*, 932–944. https://doi.org/10.4319/lo.2013.58.3.0932

Lacour, T., Larivière, J., & Babin, M. (2017). Growth, Chl *a* content, photosynthesis, and elemental composition in polar and temperate microalgae. *Limnology and Oceanography*, *62*, 43–58. https://doi.org/10.1002/lno.10369

Loeng, H. (1991). Features of the physical oceanographic conditions of the Barents Sea. *Polar Research*, *10*, 5–18. https://doi.org/10.3402/polar.v10i1.6723

Monteiro, F. M., Bach, L. T., Brownlee, C., Bown, P., Rickaby, R. E., Poulton, A. J, … Gutowska, M. A. (2016). Why marine phytoplankton calcify. *Science Advances*, *2*, e1501822. https://doi.org/10.1126/sciadv.1501822

Ormańczyk, M. R., Głuchowska, M., Olszewska, A., & Kwasniewski, S. (2017). Zooplankton structure in high latitude fjords with contrasting oceanography (Hornsund and Kongsfjorden, Spitsbergen). *Oceanologia*, *59*, 508–524. https://doi.org/10.1016/j.oceano.2017.06.003

Oziel, L., Neukermans, G., Ardyna, M., Lancelot, C., Tison, J. L., Wassmann, P, … Gascard, J. C. (2017). Role for Atlantic inflows and sea ice loss on shifting phytoplankton blooms in the Barents Sea. *Journal of Geophysical Research: Oceans*, *122*, 5121–5139.

Oziel, L., Sirven, J., & Gascard, J. C. (2016). The Barents Sea frontal zones and water masses variability (1980-2011). *Ocean Science*, *12*, 169–184. https://doi.org/10.5194/os-12-169-2016

Paasche, E. (2001). A review of the coccolithophorid Emiliania huxleyi (Prymnesiophyceae), with particular reference to growth, coccolith formation, and calcification-photosynthesis interactions. *Phycologia*, *40*, 503–529. https://doi.org/10.2216/i0031-8884-40-6-503.1

Peralta-Ferriz, C., & Woodgate, R. A. (2015). Seasonal and interannual variability of pan-Arctic surface mixed layer properties from 1979 to 2012 from hydrographic data, and the dominance of stratification for multiyear mixed layer depth shoaling. *Progress in Oceanography*, *134*, 19–53. https://doi.org/10.1016/j.pocean.2014.12.005

Pinsky, M. L., Worm, B., Fogarty, M. J., Sarmiento, J. L., & Levin, S. A. (2013). Marine taxa track local climate velocities. *Science*, *341*, 1239–1242. https://doi.org/10.1126/science.1239352

Poloczanska, E. S., Brown, C. J., Sydeman, W. J., Kiessling, W., Schoeman, D. S., Moore, P. J., ... Duarte, C. M. (2013). Global imprint of climate change on marine life. *Nature Climate Change*, *3*, 919–925. https://doi.org/10.1038/nclimate1958

Poloczanska, E. S., Burrows, M. T., Brown, C. J., García Molinos, J., Halpern, B. S., Hoegh-Guldberg, O, ... Sydeman, W. J. (2016). Responses of marine organisms to climate change across oceans. *Frontiers in Marine Science*, *3*, 62.

Polyakov, I. V., Pnyushkov, A. V., Alkire, M. B., Ashik, I. M., Baumann, T. M., Carmack, E. C, ... Krishfield, R. (2017). Greater role for Atlantic inflows on sea-ice loss in the Eurasian Basin of the Arctic Ocean. *Science*, *356*, 285–291. https://doi.org/10.1126/science.aai8204

Rey, F. (2012). Declining silicate concentrations in the Norwegian and Barents Seas. *ICES Journal of Marine Science*, *69*, 208–212. https://doi.org/10.1093/icesjms/fss007

Riebesell, U., Bach, L. T., Bellerby, R. G., Monsalve, J. R. B., Boxhammer, T., Czerny, J, ... Schulz, K. G. (2016). Competitive fitness of a predominant pelagic calcifier impaired by ocean acidification. *Nature Geoscience*, *10*, 19–23.

Slagstad, D., Wassmann, P. F. J., & Ellingsen, I. (2015). Physical constrains and productivity in the future Arctic Ocean. *Frontiers in Marine Science*, *2*, 85.

Smedsrud, L. H., Esau, I., Ingvaldsen, R. B., Eldevik, T., Haugan, P. M., Li, C, ... Risebrobakken, B. (2013). The role of the Barents Sea in the Arctic climate system. *Reviews of Geophysics*, *51*, 415–449. https://doi.org/10.1002/rog.20017

Smyth, T. J., Tyrell, T., & Tarrant, B. (2004). Time series of coccolithophore activity in the Barents Sea, from twenty years of satellite imagery. *Geophysical Research Letters*, *31*, L11302.

Tyrrell, T., Holligan, P. M., & Mobley, C. D. (1999). Optical impacts of oceanic coccolithophore blooms. *Journal of Geophysical Research: Oceans*, *104*, 3223–3241. https://doi.org/10.1029/1998jc900052

Tyrrell, T., & Merico, A. (2004). Emiliania huxleyi: Bloom observations and the conditions that induce them. In H. R. Thierstein & J. R. Young, *Coccolithophores: From molecular processes to global impact* (pp. 75–97). Berlin Heidelberg, Berlin, Heidelberg: Springer. https://doi.org/10.1007/978-3-662-06278-4

Vancoppenolle, M., Bopp, L., Madec, G., Dunne, J., Ilyina, T., Halloran, P. R., & Steiner, N. (2013). Future Arctic Ocean primary productivity from CMIP5 simulations: Uncertain outcome, but consistent mechanisms. *Global Biogeochemical Cycles*, *27*, 605–619. https://doi.org/10.1002/gbc.20055

Volent, Z., Johnsen, G., Hovland, E. K., Folkestad, A., Olsen, L. M., Tangen, K., & Sorensen, K. (2011). Improved monitoring of phytoplankton bloom dynamics in a Norwegian fjord by integrating satellite data, pigment analysis, and Ferrybox data with a coastal observation network. *Journal of Applied Remote Sensing*, *5*, 53561. https://doi.org/10.1117/1.3658032

Walczowski, W., Piechura, J., Goszczko, I., & Wieczorek, P. (2012). Changes in Atlantic water properties: An important factor in the European Arctic marine climate. *ICES Journal of Marine Science*, *69*, 864–869. https://doi.org/10.1093/icesjms/fss068

Walsh, J. J., Dieterle, D. A., Chen, F. R., Lenes, J. M., Maslowski, W., Cassano, J. J, ... Christensen, J. (2011). Trophic cascades and future harmful algal blooms within ice-free Arctic Seas north of Bering Strait: A simulation analysis. *Progress in Oceanography*, *91*, 312–343. https://doi.org/10.1016/j.pocean.2011.02.001

Wassmann, P., Kosobokova, K. N., Slagstad, D., Drinkwater, K. F., Hopcroft, R. R., Moore, S. E, ... Berge, J. (2015). The contiguous domains of Arctic Ocean advection: Trails of life and death. *Progress in Oceanography*, *139*, 42–65. https://doi.org/10.1016/j.pocean.2015.06.011

Węsławski, J. M., Buchholz, F., Głuchowska, M., & Weydmann, A. (2017). Ecosystem maturation follows the warming of the Arctic fjords. *Oceanologia*, *59*, 592–602.

Winter, A., Henderiks, J., Beaufort, L., Rickaby, R. E. M., & Brown, C. W. (2014). Poleward expansion of the coccolithophore Emiliania huxleyi. *Journal of Plankton Research*, *36*, 316–325. https://doi.org/10.1093/plankt/fbt110

Winter, A., Jordan, R. W., & Roth, P. H. (1994). Biogeography of living coccolithophores in ocean waters. In A. Winter & W. G. Siesser (Eds.), *Coccolithophores* (pp. 161–177). New York: Cambridge University Press.

SUPPORTING INFORMATION

Additional Supporting Information may be found online in the supporting information tab for this article.

Supplementary information for

Increased intrusion of warming Atlantic water leads to rapid expansion of temperate phytoplankton in the Arctic

Griet Neukermans[1,2,*] , Laurent Oziel[1], and Marcel Babin[1,2]

[1]Takuvik Joint International Laboratory, CNRS and Université Laval, 1045 Avenue de la Médecine, G1V0A6 Québec, Canada

[2]Sorbonne Université, Centre National de la Recherche Scientifique (CNRS), Laboratoire d'Océanographie de Villefranche (LOV), 06 230 Villefranche-sur-Mer, France

*Corresponding author: OOV-LOV, 181 Chemin du Lazaret, 06230 Villefranche-sur-Mer, France, griet.neukermans@obs-vlfr.fr

Supplementary methods and results

Validation of water mass classification

To validate the remote sensing-based water mass classification we used one of the most complete hydrographic in situ collections of the Barents Sea with over 130 000 profiles of temperature and salinity collected between 1980 and 2012 (Oziel *et al.*, 2016). We intersected the remotely sensed water mass classification with the in situ surface data in winter over the 1998-2012 time period. The resulting potential temperature (θ)−salinity (S) diagram in Supplementary Fig. S3 shows good correspondence between the remote and in situ water mass definitions. Most of the in situ data identified as ArW fall within theoretical θ–S boundaries for Arctic waters, which are typically defined as waters with temperatures below 0 °C and S between 34.0 and 34.7 PSU, depending on the study (Oziel *et al.*, 2016),(Loeng, 1991). About half of the in situ data identified as AW fall within theoretical θ–S boundaries for Atlantic waters, whereas the other half corresponds to Norwegian coastal water which have lower salinities than Atlantic-origin waters and cannot be differentiated from each other by remote sensing of SST alone. The PFW fall in between as they represent a zone where Atlantic and Arctic water masses meet and mix.

Next, we examined the seasonal stability of the temperature front for which we used the SINMOD (SINtef Ocean MODel) model (Slagstad *et al.*, 1999). This is a coupled 3-D hydrodynamic and bio-geochemical model that has been under continuous development, assessment, and validation in the Barents Sea over the past 30 years (Slagstad *et al.*, 1999, 2015; Slagstad & McClimans, 2005; Ellingsen *et al.*, 2009; Oziel *et al.*, 2016). Here, we analyzed the high spatial resolution output at 4 km resolution and applied the same local variance filter and Polar Front detection methods as for the remote sensing data. This analysis shows that overall the seasonal variability of the temperature front is weak (supplementary Fig. S1). In some years differences were found which may be attributed

to unrealistic summer heat and volume transport and/or warming by the atmosphere. The model also shows interannual variability of the position of the front with a more northward position during warm years (2000-2002, 2005-2008, 2012) compared to colder years (1998-1999, 2003-2004, 2009-2011), which is in agreement with interannual variability of its position obtained from remote sensing data. Even though the SINMOD model accurately represents seasonal variations, it is unable to reproduce climatic trends (Ellingsen *et al.*, 2009; Slagstad *et al.*, 2015), which is why we used the position of the front obtained from remote sensing.

Calculation of mean PAR in the mixed-layer

The mean photosynthetically available radiation, PAR, in the mixed-layer was obtained using the following formula:

$$PAR_{ML} = \frac{1}{MLD}\int_{0}^{MLD} PAR(0-)\exp\left(-K_{PAR}\, z\right) dz$$

where MLD is the depth of the mixed layer (see Methods), $PAR(0-)$ is the photosynthetically available radiation just below the ocean surface and K_{PAR} is its diffuse attenuation coefficient obtained from the depth of the euphotic zone, Z_{eu}as:

$$K_{PAR} = \frac{-\log\left(0.01\right)}{Z_{eu}}$$

where $PAR(0-)$ and Z_{eu} are obtained from NASA's standard daily level 3 products from the SeaWiFS (1998-2007, 9.2 km spatial resolution) and MODIS (2003-2016, 4.6 km spatial resolution) ocean colour sensors, downloaded from NASA's ocean colour website (http://oceandata.sci.gsfc.nasa.gov).

Correlation analyses between maximum summer PIC and PAR_{ML} in summer is shown in Supplementary Table S4.

Supplementary Figures

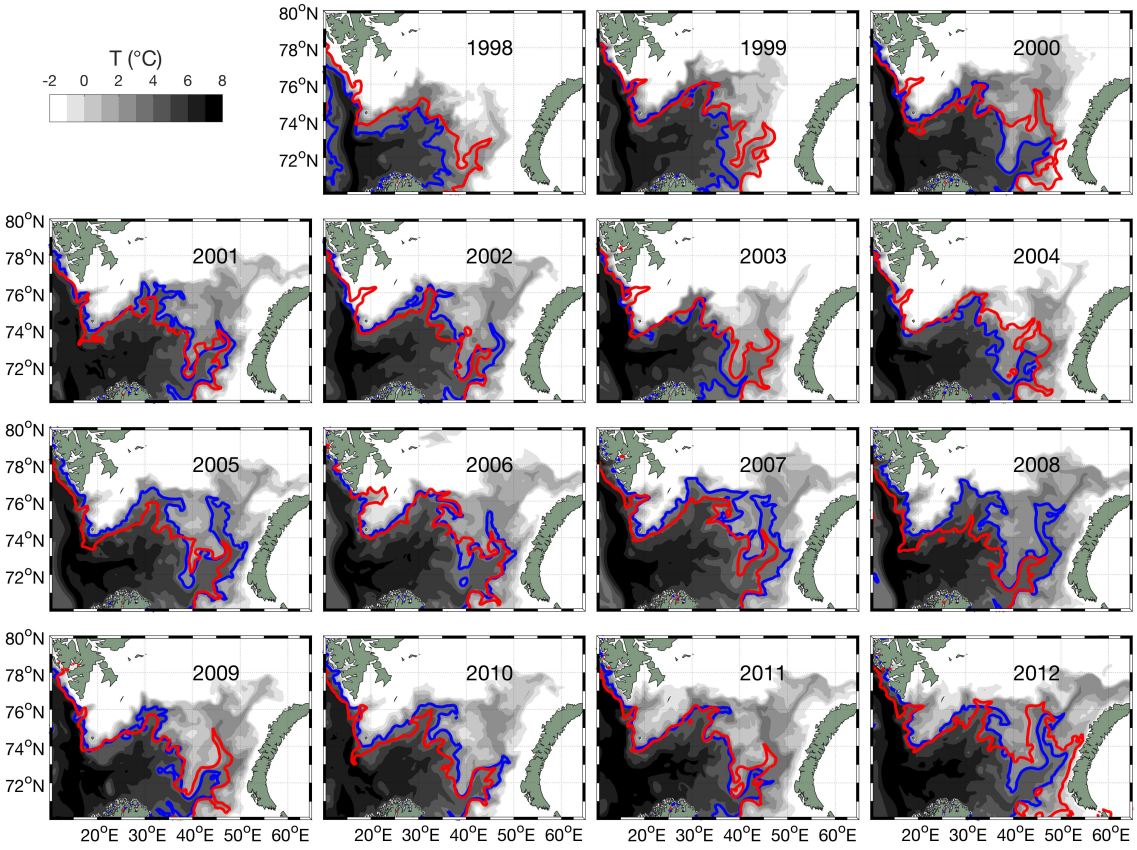

Supplementary Figure S1. SINMOD model output analysis of winter temperature fields with surface winter (blue) and sub-surface (30m) summer (red) southern edge of the Polar Front.

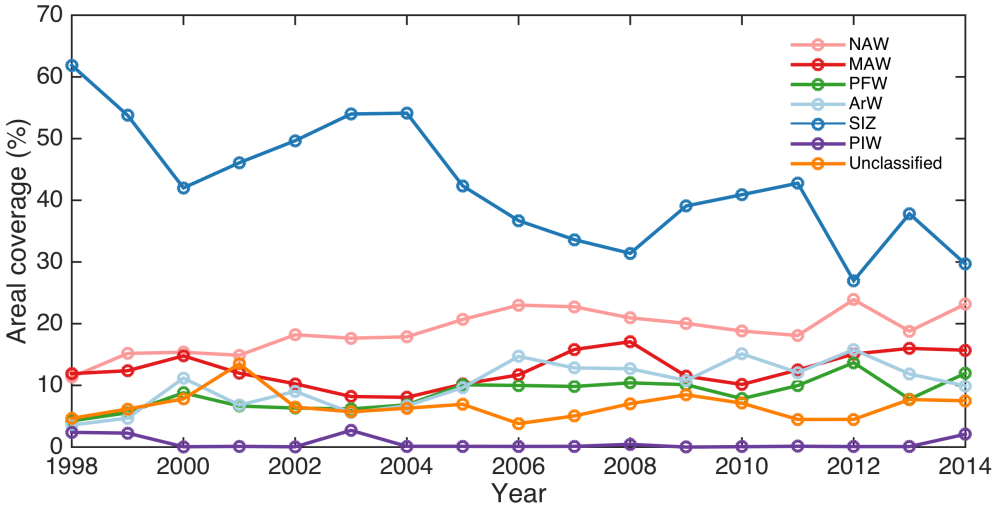

Supplementary Figure S2. Areal coverage of water masses in the Barents Sea based on remotely sensed data of sea surface temperature (Baker-Yeboah, Sheekela; Saha, Korak; Zhang, Dexin; Casey, Kenneth S.; Kilpatrick, Katherine A.; Evans, Robert H.; Ryan, 2016) and ice cover (Cavalieri, D., Parkinson, C., Gloersen, P., Zwally, 1996). See methods for details. Pixels with no valid remotely sensed SST observation in March/April are unclassified.

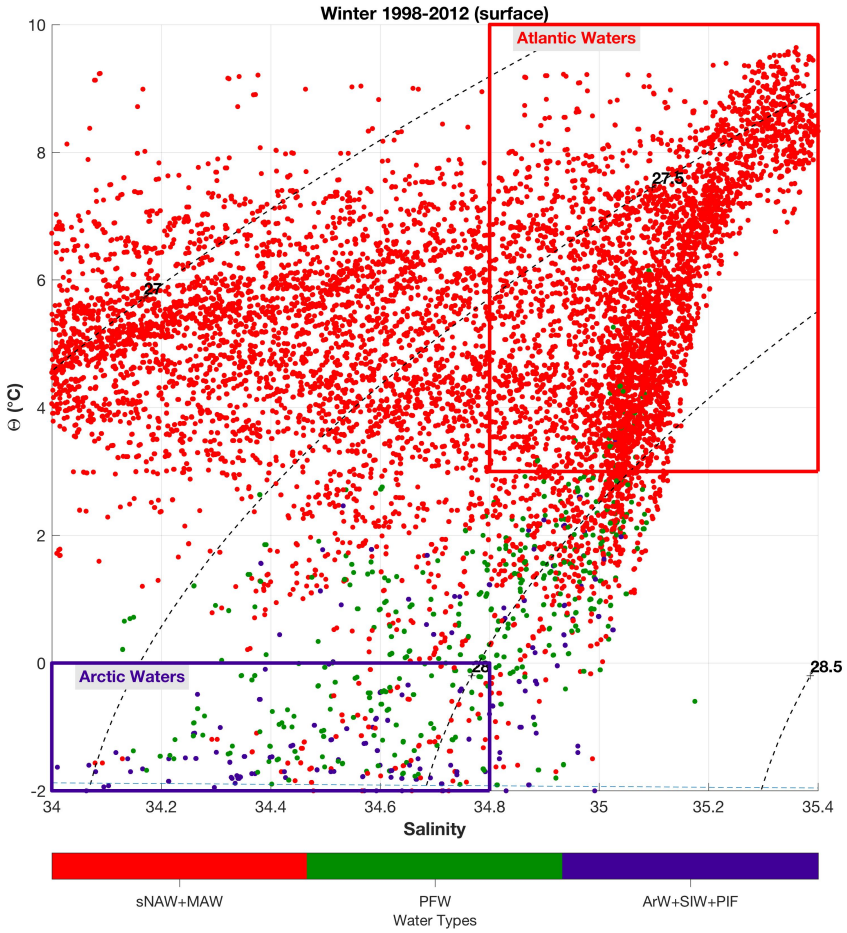

Supplementary Figure S3. Potential temperature (θ)−salinity (S) diagram diagram of winter surface in situ data (1998-2012) and corresponding water masses obtained from remote sensing. Boxes represent the theoretical definitions of ideal Arctic and Atlantic Waters from the literature (1, 2 and references therein). Dashed lines are isopycnals with potential density anomalies in kg/m^3.

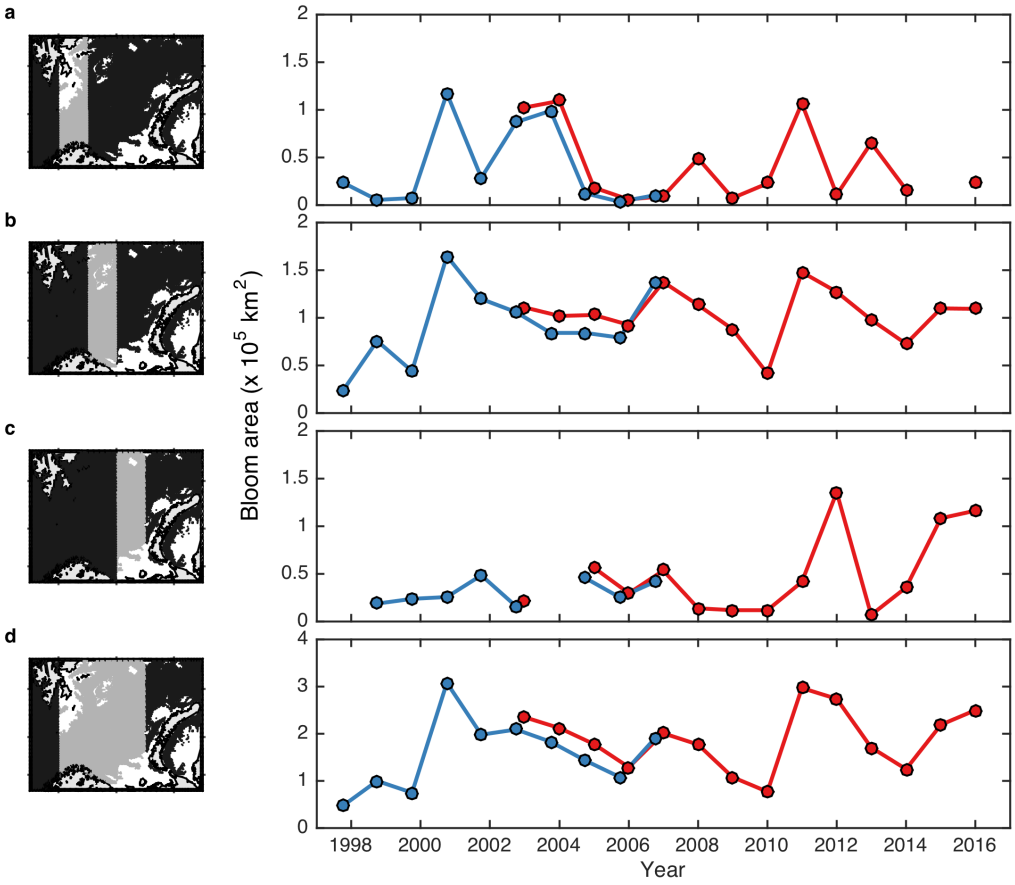

Supplementary Figure S4. Interannual changes in the distribution area of *E. huxleyi* blooms (PIC>0.006 mol m^{-3}) with PIC obtained from SeaWiFS (blue) and MODIS (red) ocean colour sensors.

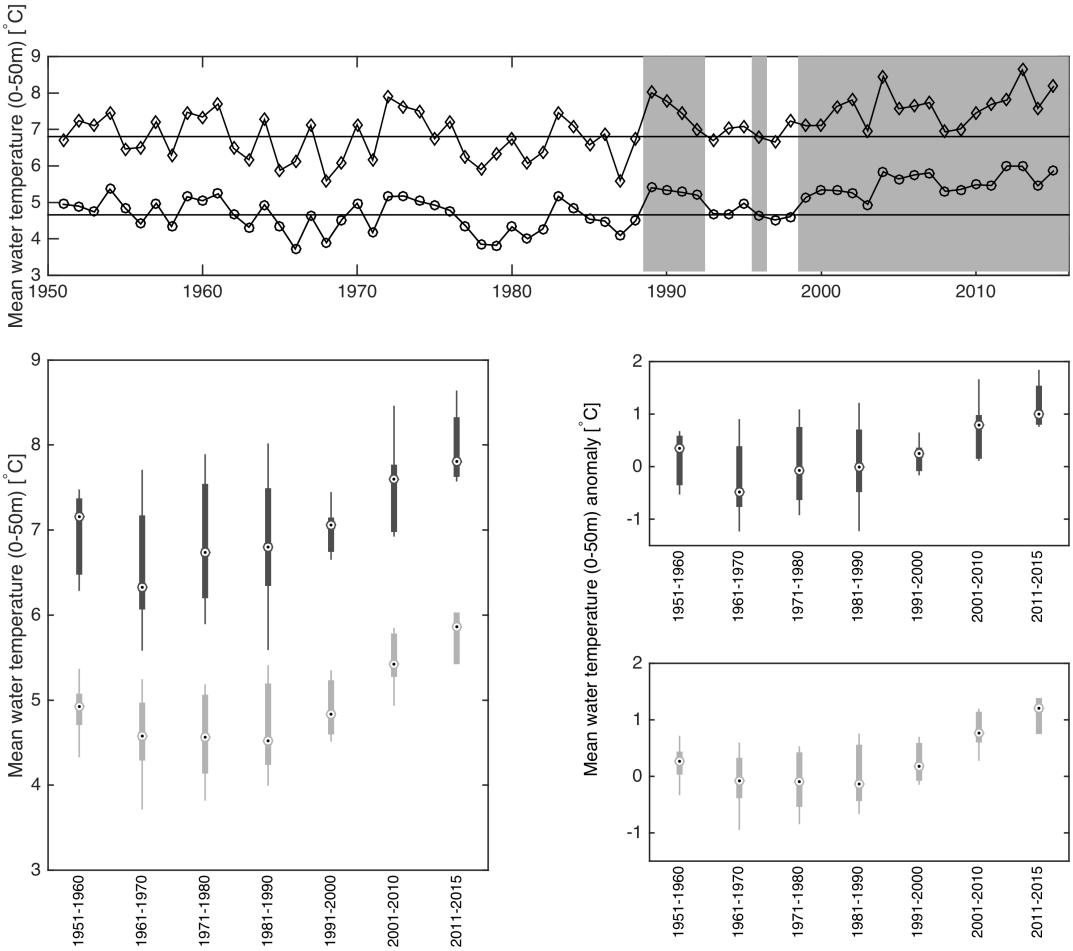

Supplemental Figure S5. Long-term trends in annual (circles, light grey) and summer (diamonds, dark grey) mean temperature in the top 50 m of the water column on the main branch of the Atlantic water current on the Kola hydrographic section (Knipovich Polar Research Institute of Marine Fisheries and Oceanography (PINRO)). Shaded grey areas in top panel indicate presence of *E. huxleyi* blooms in the Barents Sea (Smyth *et al.*, 2004).

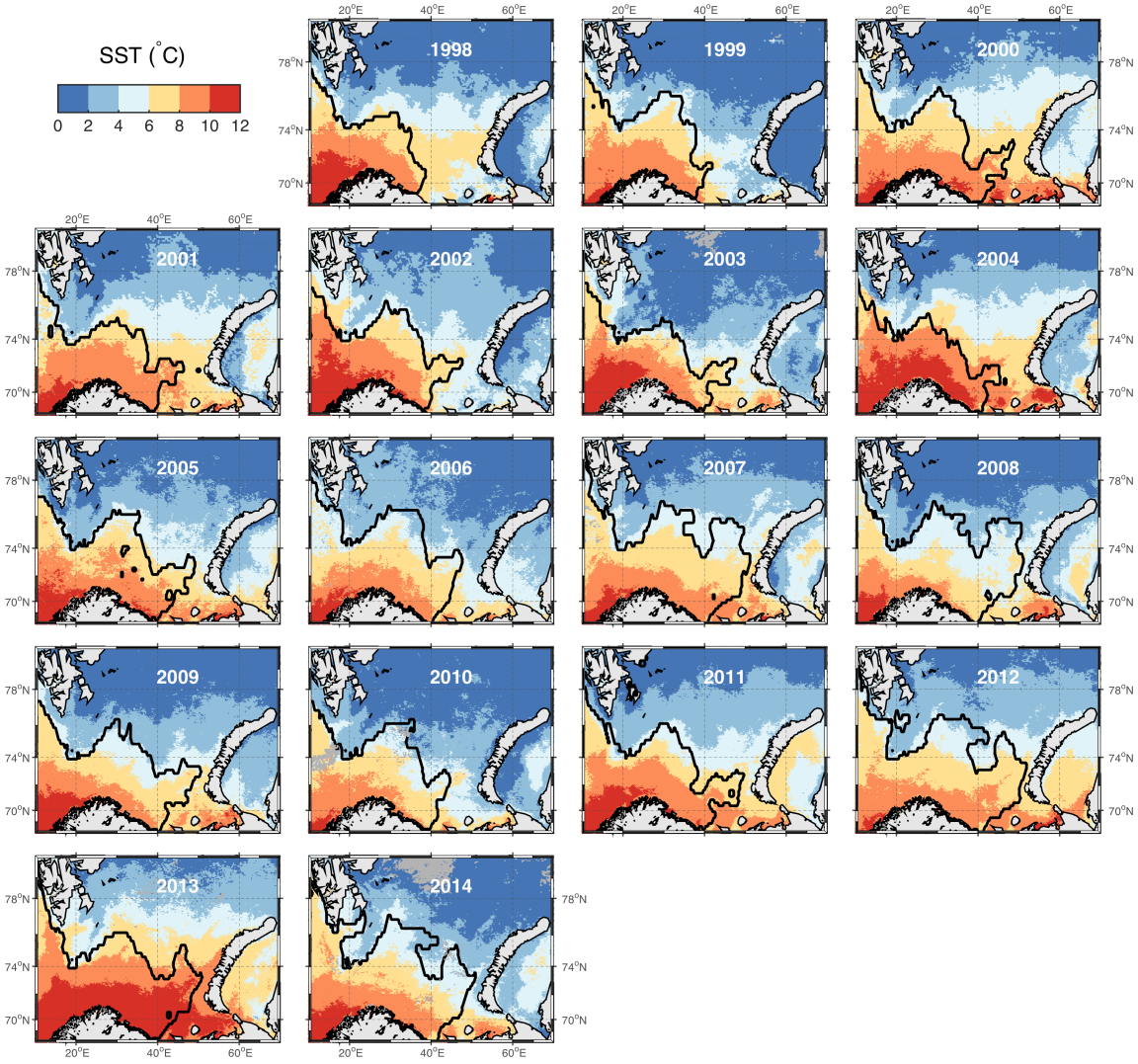

Supplementary Figure S6. Remotely sensed summer mean SST from the AVHRR sensor(Baker-Yeboah, Sheekela; Saha, Korak; Zhang, Dexin; Casey, Kenneth S.; Kilpatrick, Katherine A.; Evans, Robert H.; Ryan, 2016) with black line indicating the extent of Atlantic Waters.

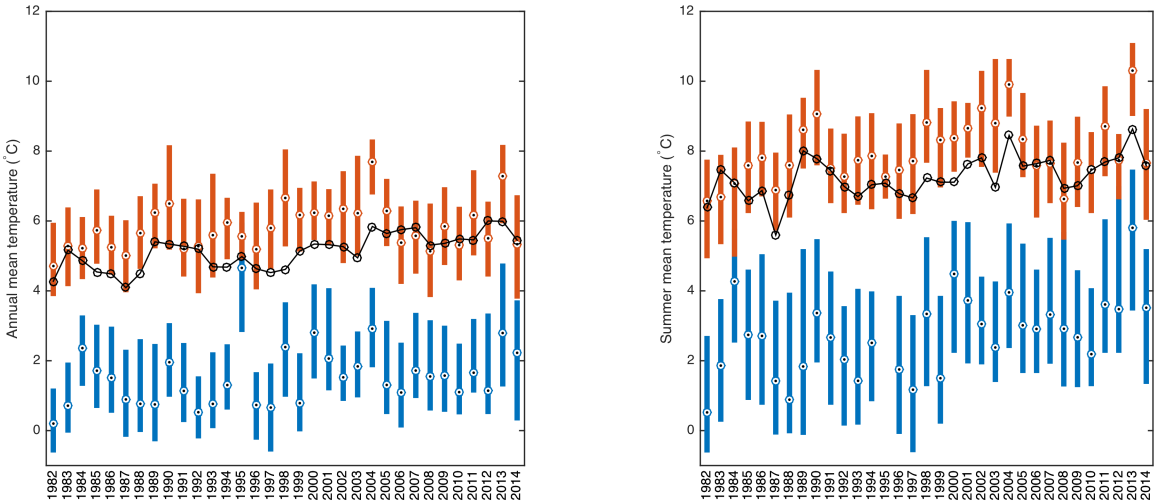

Supplementary Figure S7. Interannual changes in (a) annual and (b) summer (July-Sep) mean SST in Atlantic (red) and Arctic (blue) water masses of the Barents Sea over the period 1982-2014. Boxes extend from the 25th to the 75th percentile of remotely sensed SST within each water mass, with circles representing median values. Black line represents temperature data (0-50 m) on the Kola hydrographic section (Knipovich Polar Research Institute of Marine Fisheries and Oceanography (PINRO)). Regression coefficients and statistics for each time series are shown in Supplementary Table S2.

Supplementary Tables

Supplementary Table S1. Coefficient estimates and statistics of linear regression analyses of annual mean and summer mean surface temperature over the time period 1982-2014 in various water masses of the Barents Sea. 95% confidence intervals are given for Pearson's product moment correlation coefficient *r* , and for the slope and offset of the linear regression, as *dr, doffset* and *dslope*, respectively. Temperature data (shown in Supplementary Fig. S5) are remotely sensed spatial means for each water mass domain, whereas Kola data is vertically integrated temperature data (0-50m) on the Kola transect stations on the main branch of the Atlantic water current (Knipovich Polar Research Institute of Marine Fisheries and Oceanography (PINRO)). Significance of results for each dataset are indicated as follows: *** for $p < 0.001$; ** for $p < 0.01$; * for $p < 0.05$.

	Water mass	*r*	*dr*	*p*	*offset*	*slope*	*doff*	*dslope*	*F*	
Annual Mean T	Arctic	0.395	0.341	0.025	-56.075	0.029	49.935	0.025	5.536	*
	Atlantic	0.349	0.342	0.046	-41.237	0.024	46.214	0.023	4.310	*
	NAW	0.261	0.351	0.142					2.269	
	Kola	0.725	0.217	0.000	-70.527	0.038	26.365	0.013	34.254	***
Summer Mean T	Arctic	0.506	0.315	0.003	-114.189	0.059	74.262	0.037	10.337	**
	Atlantic	0.397	0.335	0.022	-64.855	0.036	61.736	0.031	5.786	*
	NAW	0.367	0.340	0.035	-56.022	0.032	59.948	0.030	4.839	*
	Kola	0.533	0.301	0.001	-58.945	0.033	38.502	0.019	12.299	**

Supplementary Table S1. 16^{th}, 50^{th}, and 84^{th} percentiles of sea surface temperatures of Polar Front waters based on remote sensing data from the AVHRR sensor (Baker-Yeboah, Sheekela; Saha, Korak; Zhang, Dexin; Casey, Kenneth S.; Kilpatrick, Katherine A.; Evans, Robert H.; Ryan, 2016), 1982-2014.

Year	P16 (SST)	Median SST	P84 (SST)
1982	-0.560	-0.027	0.518
1983	-0.450	-0.017	0.435
1984	-0.506	-0.004	0.489
1985	-0.621	0.005	0.595
1986	-0.391	0.002	0.399
1987	-0.524	-0.037	0.450
1988	-0.464	0.003	0.405
1989	-0.479	0.003	0.484
1990	-0.529	-0.004	0.569
1991	-0.520	-0.036	0.588
1992	-0.458	-0.003	0.482
1993	-0.480	0.050	0.611
1994	-0.542	0.002	0.591
1995	-0.520	0.036	0.303
1996	-0.384	-0.005	0.371
1997	-0.575	-0.007	0.541
1998	-0.414	0.020	0.521
1999	-0.518	-0.008	0.444
2000	-0.442	0.029	0.556
2001	-0.514	-0.037	0.487
2002	-0.495	0.002	0.546
2003	-0.491	0.015	0.611
2004	-0.602	0.005	0.593
2005	-0.391	0.005	0.579
2006	-0.335	-0.009	0.375
2007	-0.434	-0.001	0.436
2003	-0.456	0.014	0.600
2004	-0.557	-0.003	0.604
2005	-0.485	-0.018	0.621
2006	-0.346	0.005	0.415
2007	-0.403	0.002	0.426
2008	-0.383	0.008	0.470
2009	-0.465	0.014	0.622
2010	-0.484	0.002	0.454
2011	-0.478	-0.004	0.490
2012	-0.480	0.004	0.543
2013	-0.318	0.007	0.359
2014	-0.438	0.013	0.439

Supplementary Table S3. Coefficient estimates and statistics of linear regression analyses of *E. huxleyi* bloom leading edge latitudinal position over the time period 1989-2016, shown in Fig. 3. 95% confidence intervals are given for Pearson's product moment correlation coefficient *r*, and for the slope and offset of the linear regression, as *dr, doffset* and *dslope,* respectively.

Longitude sector	*r*	*dr*	*p*	*offset*	*slope*	*doffset*	*dslope*	*F*	
20E-30E	0.149	0.463	0.532	74.214	0.026	1.622	0.084	0.406	
30E-40E	0.452	0.403	0.031	72.987	0.067	1.141	0.060	5.381	*
40E-50E	0.663	0.364	0.002	71.177	0.104	1.212	0.060	13.318	**

Supplementary Table S4. Correlation analyses between maximum summer PIC and environmental drivers. *n* is the number of observations, *r* is Pearson's product moment correlation coefficient with 95% confidence interval, *dr*.

	n	*r*	*dr*	*p*	
summer PAR in ML	60	0.395	0.238	0.002	**
summer MLD	60	-0.511	0.166	0.000	***

Author contributions

G.N. and M.B. conceptualized the study. G.N. developed the scientific approach, analyzed and interpreted the data, performed statistical analyses, produced tables and figures, and wrote the manuscript. L.O. contributed analyses in physical oceanography presented in Supplementary Figures S6-S7. All authors discussed results and commented on earlier versions of the manuscript.

Supplementary references

Baker-Yeboah, Sheekela; Saha, Korak; Zhang, Dexin; Casey, Kenneth S.; Kilpatrick, Katherine A.; Evans, Robert H.; Ryan T (2016) AVHRR Pathfinder version 5.3 level 3 collated (L3C) global 4km sea surface temperature.

Cavalieri, D., Parkinson, C., Gloersen, P., Zwally H (1996) Sea Ice Concentrations from Nimbus-7 SMMR and DMSP SSM/I-SSMIS Passive Microwave Data, Version 1.

Ellingsen I, Slagstad D, Sundfjord A (2009) Modification of water masses in the Barents Sea and its coupling to ice dynamics: a model study. *Ocean Dynamics*, **59**, 1095–1108.

Knipovich Polar Research Institute of Marine Fisheries and Oceanography (PINRO) Kola section hydrographic data set.

Loeng H (1991) Features of the physical oceanographic conditions of the Barents Sea. *Polar Research*, **10**, 5–18.

Oziel L, Sirven J, Gascard JC (2016) The Barents Sea frontal zones and water masses variability (1980-2011). *Ocean Science*, **12**, 169–184.

Slagstad D, McClimans TA (2005) Modeling the ecosystem dynamics of the Barents sea including the marginal ice zone: I. Physical and chemical oceanography. *Journal of Marine Systems*, **58**, 1–18.

Slagstad D, Downing K, Carlotti F, Hirche H-J (1999) Modelling the carbon export and air–sea flux of CO2 in the Greenland Sea. *Deep Sea Research Part II: Topical Studies in Oceanography*, **46**, 1511–1530.

Slagstad D, Wassmann PFJ, Ellingsen I (2015) Physical constrains and productivity in the future Arctic Ocean. *Frontiers in Marine Science*, **2**, 85.

Smyth TJ, Tyrell T, Tarrant B (2004) Time series of coccolithophore activity in the Barents Sea, from twenty years of satellite imagery. *Geophysical Research Letters*,

31, L11302.